Fluid-Wall Effectiveness for Preventing Oxidation in Solar-Thermal ZnO Reactors

Christopher Perkins, Paul Lichty, and Alan W. Weimer
Dept. of Chemical and Biological Engineering, University of Colorado at Boulder, Boulder, CO 80309

Carl Bingham
Concentrating Solar Power Group, National Renewable Energy Laboratory, Golden, CO 80401

DOI 10.1002/aic.11203
Published online May 14, 2007 in Wiley InterScience (www.interscience.wiley.com).

Computational fluid dynamics simulations of a "fluid-wall" solar reactor for the dissociation of ZnO were performed to determine the effectiveness of the fluid-wall strategy at preventing oxygen from reacting with the reactor wall. An axial boundary layer near the porous wall was found to exist where ZnO concentrations were essentially zero, demonstrating that the concept was effective at preventing particle contact with the reactor wall. ZnO particles were found to heat nearly instantaneously (>10^5 K/s), and ZnO conversions were found to be significant (>50%) in the short residence times employed. Conditions for high levels of oxidation of the tube wall coincided with those for high levels of ZnO conversion, and oxidation levels were high (>50%). This was confirmed in solar experiments, where all oxygen products reacted with the tube wall. Although an effective concept for keeping particles from contacting the wall, the fluid-wall strategy was not effective for preventing oxidation. © 2007 American Institute of Chemical Engineers *AIChE J*, 53: 1830–1844, 2007
Keywords: energy, mathematical modeling, fluid mechanics, solar, fluid-wall

Introduction and Background

The Zn/ZnO thermochemical water splitting cycle offers a promising pathway to renewable hydrogen production through the utilization of concentrated solar energy. The cycle consists of two chemical steps. In the first step, ZnO is dissociated at ultra-high temperatures (1600–1900°C):

$$\mathrm{ZnO} \rightarrow \mathrm{Zn} + \frac{1}{2}\mathrm{O_2} \tag{1}$$

This reaction is highly endothermic ($\Delta H_T^\circ = 450$ kJ/mol), and the necessary energy is supplied thermally from concentrated solar sources.[1] In a second, nonsolar step, the product zinc metal is combined with water:

$$\mathrm{Zn} + \mathrm{H_2O} \rightarrow \mathrm{ZnO} + \mathrm{H_2} \tag{2}$$

This reaction is exothermic ($\Delta H_T^\circ = -130$ kJ/mol), and can be performed continuously with stored zinc product from the first step. This effectively solves the inherent intermittent energy source problems associated with the diurnal nature of solar energy. The zinc oxide from the second reaction can be recycled to the first reaction, completing a closed zinc cycle. The net reaction is the dissociation of water to form hydrogen and oxygen.

With such high operating temperatures for the first reaction in the cycle, a key concern is the selection or engineering of a suitable material of reactor construction. Such a material must have excellent thermal properties: high temperature resistance, good thermal shock resistance, and the ability to

Correspondence concerning this article should be addressed to C. Perkins at christopher.perkins@colorado.edu.

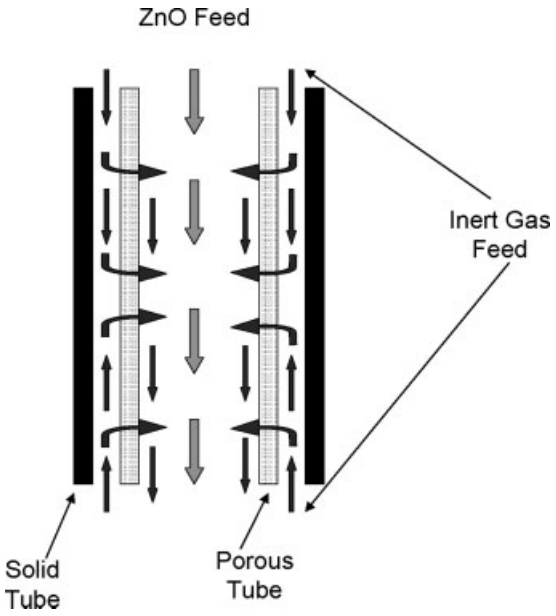

Figure 1. Fluid wall concept for protection of reactor wall from corrosive oxidation.

withstand high thermal gradients. Additionally, the material must be oxidation resistant at ultra-high temperatures since oxygen is a product of the first reaction step. Unfortunately, such a material is currently unknown. Further, the list of known materials with the appropriate thermal properties is short, consisting mostly of graphite, carbides, and carbon-based composites.

If it were possible to protect the reactive tube wall from oxygen, then the use of these carbon-based materials could become an option. One method to achieve such a goal is the creation of a "fluid wall" diffusion barrier. This method has been used to prevent carbon particle deposition on tube walls in solar methane dissociation,[2] as well as prevention of particle contact during high temperature carbothermal reduction reactions.[3] The "fluid wall" can be created in a tubular reactor by the coaxial insertion of a smaller diameter porous tube of high temperature material into the solid reactor tube. (Figure 1) The main reactants (in this case, ZnO particles) are flowed as an aerosol through the inner region of this porous tube. In the annular region, inert gas can be flowed from both top and bottom. The resulting pressure difference across the porous tube forces the inert gas radially through it and into the main flow channel. In theory, this reduces the concentration of particles and oxygen near the wall by effusion, limiting the extent of oxidation of the porous reactor wall.

Computational fluid dynamics (CFD) simulations can be of great aid in determining the viability and design parameters for such a system. By solving the governing physical equations involved, the extent of wall reaction can be studied for a large number of geometrical configurations, flow parameters, and porous wall properties. Simulations of such a situation can give an indication of how viable the "ideal" situation is in terms of the extent of wall reaction. They can also help to identify optimal points for reactor design, and the number of much more costly experimental studies used to verify these conclusions can be minimized.

2D axisymmetric CFD simulations with these goals were performed using COMSOL multiphysics over an array of physical factors.[4] The commercial software employed uses a finite element method to solve the governing physical equations. The physical factors were chosen to determine the effectiveness of the fluid wall approach for preventing corrosive oxidation of the reactor wall. The results of the simulations were confirmed in "on-sun" solar experiments.

Model Geometry and Governing Equations

The model consisted of the governing momentum, energy, and mass transfer partial differential equations for a tubular fluid-wall solar receiver/reactor. The base model geometry is shown in Figure 2. The central flow region was defined by the inner diameter of the porous tube, which was set to 2.286 cm (0.9″). The porous tube itself was specified to be 0.254 cm (0.1″) thick, giving an outer diameter of 2.794 cm (1.1″). The annular section was defined by the outer diameter of the porous tube and the inner diameter of the solid containing tube, which was set to 3.302 cm (1.3″). These dimensions were very similar to those in fluid-wall reactors employed at the National Renewable Energy Laboratory by Dahl et al.[2] for the study of thermal methane dissociation.

The governing momentum balance in the central and annular flow regions was:

$$\nabla \cdot \rho \vec{v} = 0 \tag{3}$$

$$-(\nabla \cdot \rho \vec{v}\,\vec{v}) - \nabla p - (\nabla \cdot \vec{\vec{\tau}}) + \rho_{\text{eff}} \vec{g} = 0 \tag{4}$$

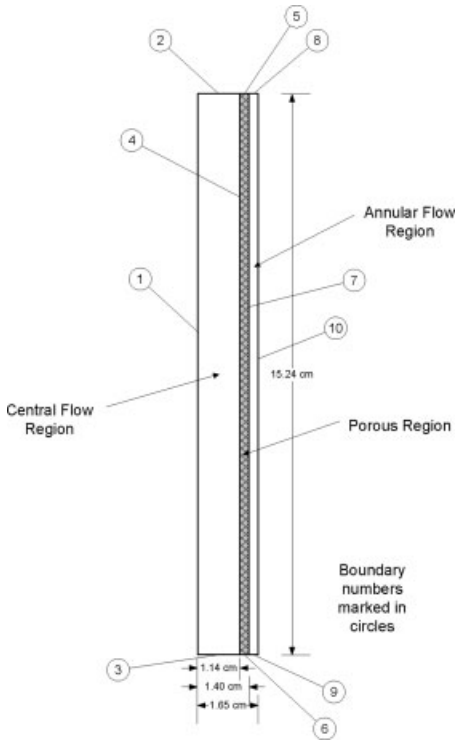

Figure 2. Fluid wall reactor model geometry and boundary conditions.

$$\vec{\vec{\tau}}_{ij} = -\mu\left(\frac{\partial v_i}{\partial x_j} + \frac{\partial v_j}{\partial x_i}\right) + \frac{2}{3}\mu(\nabla \cdot \vec{v})\delta_{ij} \tag{5}$$

where ρ is the gas density, $\vec{v}$ is the velocity vector, p is the gas pressure, $\vec{\vec{\tau}}$ is the viscous stress tensor, $\vec{g}$ is the gravitational force vector, δ_{ij} is the Kronecker delta, and μ is the viscosity of the gas. The flow was assumed to be azimuthally symmetric and at steady state, and all angular and time-dependent terms were set to zero in arriving at Eqs. 3–5.

The carrier gas for the aerosol phase and the inert gas in the annular region simulations was assumed to be argon. Properties for the gas were taken from the CRC Handbook of Chemistry and Physics.[5] The density was calculated locally using the ideal gas law. Calculation of the viscosity and thermal conductivity of the gas at elevated temperatures was done using Chapman-Enskog models, as described in Bird et al.:[6]

$$\mu = 2.6693 \times 10^{-6}\frac{\sqrt{MT}}{\sigma^2\Omega} \tag{6}$$

$$k = 0.0833\sqrt{\frac{T/M}{\sigma^2\Omega}} \tag{7}$$

where σ is the characteristic diameter of the molecule, Ω is the viscosity–thermal conductivity collision integral, T is the gas temperature, and M is the molecular weight. The viscosity μ is given by this equation in kg m^{-1} s^{-1}, and the thermal conductivity k in W m^{-1} K^{-1}.[6]

The ZnO particles were not treated as a separate phase in calculation of the velocity profiles within the reactor. For a homogenous distribution of ZnO particles 1 μm in diameter traveling through a 2.29 cm inner diameter tube in 1 SLPM of Argon gas, the Stokes number is between 1×10^{-4} and 1×10^{-2}. As this $St \ll 1$, the particles can be assumed to move with the gas streamlines, and a separate momentum balance would be superfluous.[7]

In the porous region, the steady-state Brinkman equation was used:

$$-\nabla \cdot \mu(\nabla\vec{v} + (\nabla\vec{v})^T) + \left(\frac{\mu}{k_p}\vec{v} + \nabla p\right) = 0 \tag{8}$$

$$\nabla \cdot \vec{v} = 0 \tag{9}$$

This is a modified Darcy law expression that accounts for viscous momentum transport in the gas phase. The Darcy law portion of the expression relates the velocity in the gas phase to the pressure gradient by the proportionality factor k_p/μ. The factor k_p, known as the permeability, is defined by this linear Darcy relationship, and it is typically a function of porous material properties (pore size, void fraction) and gas properties. Values for k typically range between 1×10^{-8} and 1×10^{-13} m^2, and the model studies were performed for permeabilities within this range.[8] The Brinkman equation is only valid for low flow regimes, where particle Reynolds numbers are lower than about 0.1.[9] In this system, the particle Reynolds numbers range between 3×10^{-5} and 3×10^{-2} depending on the size of the particles that constitute the porous region. These are well within the range of applicability for the Brinkman equation.

The energy balance used for the gas phase in the central and annular flow regions was:

$$-(\nabla \cdot \rho C_p T\vec{v}) - (\nabla \cdot \vec{q}) + (\vec{v} \cdot \nabla p) + Q_{part} = 0 \tag{10}$$

$$\vec{q} = -k\nabla T \tag{11}$$

where C_p is the heat capacity of the gas and $\vec{q}$ is the conductive heat flux. Viscous heating effects were ignored and steady-state was assumed in arriving at Eqs. 10 and 11.

The source term, Q_{part}, was a volumetric source term for heating of the gas because of conduction from the particle phase. This term was not included in the annular region, as the particles were not permitted to flow through the porous region. The details of the formulation of this term are described below when the energy balance for the particle phase is discussed.

In the porous region, the energy balance was:

$$-(\nabla \cdot \rho C_p T\vec{v}) - (\nabla \cdot \vec{q}) + (\vec{v} \cdot \nabla p) + Q_{porous} = 0 \tag{12}$$

$$\vec{q} = -k\nabla T \tag{13}$$

This is identical to that for the central region, except that $Q_{particle}$ has been replaced by Q_{porous}. As the particles were not permitted in the porous flow region, there was obviously no conductive heat transfer between the particles and the gas. Q_{porous} was defined as the energy transfer from the porous medium to the gas flowing through it. To determine this heat transfer, the temperature of the porous medium must either be known or solved for.

The energy received by the porous medium by radiation from the outer tube wall was:

$$Q_{rad,in} = A_{porous}\varepsilon_{porous}\sigma_{sb}T_{wall}^4 \tag{14}$$

where A_{porous} is the outer lateral surface area of the porous medium, ε_{porous} is the emissivity of the porous medium, σ is the Stefan–Boltzmann constant, and T_{wall} is the outer wall temperature. For a typical wall temperature, 2000 K, this energy input would be 12.1 kW. The energy required to heat the gas phase to the wall temperature was:

$$Q_{gas,tot} = \dot{n}_{gas}\int_{T_0}^{T_{wall}} C_{p,gas}dT \tag{15}$$

where $\dot{n}_{gas}$ is the molar gas flowrate and $C_{p,gas}$ is the molar heat capacity of the gas. The energy required to heat the ZnO particle phase to the wall temperature and then dissociate the ZnO was:

$$Q_{part,tot} = \dot{n}_{ZnO,in}\left(\int_{T_0}^{T_{wall}} C_{p,part}dT + \Delta H_T^\circ\right) \tag{16}$$

where $\dot{n}_{part}$ is the molar flowrate of ZnO particles, $C_{p,part}$ is the molar heat capacity of the particles, and ΔH_T° is the standard molar enthalpy of dissociation of ZnO. For the highest particle flowrate examined (2 g/min) and the highest total gas flow (3 SLPM), these values are 78.97 and 212.5 W for the gas and particle phase, respectively. This gives a total

energy requirement that is about 2.5% of the total energy received by the porous tube. When considering that the particles would not even flow through the porous region, the heating requirement becomes less than 0.7% of the total energy. Therefore, it was safe to assume that the porous tube had a steady-state temperature that was equal to that of the outer tube wall. The outer tube temperature, T_{wall}, was then used in the determination of Q_{porous}.

To model the heat transfer from the porous medium to the gas phase, the porous phase was treated as a packed bed of particles with the inert gas passing through the interstices. The heat transfer from these "particles" to the gas was then given by a film transfer expression:

$$Q_{porous} = h_{porous} A_{part,vol} (T_{wall} - T) \tag{17}$$

where h_{porous} is the film transfer coefficient and $A_{part,vol}$ is the surface area to volume ratio of the "particles" chosen for the packed bed model of the porous medium. This was calculated by assuming spherical particles 1 mm in diameter. The effects of this assumption on the model solution were explored and are discussed below. The film transfer coefficient was given by Kaviany:[10]

$$h_{porous} = \left[\frac{k_{porous}}{d_{part,porous}}\right]\left[\frac{1-\varepsilon}{\varepsilon}\right]\left[0.5Re_p^{1/2} + 0.2Re_p^{2/3}\right]Pr^{1/3} \tag{18}$$

where k_{porous} is the thermal conductivity of the permeable material, given as 0.58 W m^{-1} K^{-1}. This is the extrapolated thermal conductivity of Crystar® porous silicon carbide, a candidate material for use in high temperature fluid wall reactors.[11] $D_{part,porous}$ is the diameter of the virtual particles used in the packed bed model of the porous material, and ε is the void fraction in that packed bed. Re_p is the particle Reynolds number, and Pr is the Prandtl number for the gas.

The mass balance for the ZnO particle phase was given by the continuity equation:

$$\nabla \cdot (-D_{ZnO-Ar} \nabla c_{ZnO} + c_{ZnO} \vec{v}) = R_{ZnO} \tag{19}$$

where c_{ZnO} is the concentration of ZnO particles in the gas, D_{ZnO-Ar} is the diffusion coefficient of ZnO in argon gas, and R_{ZnO} is the volumetric reaction rate for the dissociation of ZnO. This amounted to a "smearing out" of the particle phase for mass transfer purposes, turning what was really a discrete particle tracking problem into a continuous problem. This is not an issue so long as the particle flow through the tube is relatively equally dispersed and the particles move at the velocity of the gas phase. For simplicity of the simulation, the even dispersion was assumed, and the justification for the coupling of the particle flow to the gas velocity was described above. The volumetric rate, R_{ZnO}, was calculated for an experimentally determined L'vov type model:[12]

$$R_{ZnO} = -k_0 e^{\frac{-E_a}{RT}} (1-X)^{2/3} \tag{20}$$

$$k_0 = \frac{N_A D_{O_2-Ar}^{1/2} D_{Zn-Ar}^{1/2}}{qzRT} e^{\frac{\Delta S_T^\circ}{vR}} \tag{21}$$

$$E_a = \frac{\Delta H_T^\circ}{v} \tag{22}$$

In the above equations, N_A is Avogadro's number, D_{O_2-Ar} and D_{Zn-Ar} are the diffusion coefficients of oxygen and zinc in argon, respectively, q is the number of atoms of Zn per unit surface area of solid, z is the diffusion distance from the surface to the bulk gas, v is the number of moles of gas generated by dissociation of one mole of solid, ΔS_T is the standard entropy of dissociation for the solid at temperature T, ΔH_T is the standard enthalpy of dissociation for the solid at temperature T, R is the gas constant, and X is the fractional conversion of solid. For dissociation of ZnO, E_a = 356 kJ/mol, ΔH_T° = 724.5 kJ/mol at 2000 K, $q = 1 \times 10^{-17}$ m^{-2}, ΔS_T° = 266.6 J mol^{-1} K^{-1} at 2000 K, v = 2, and z was varied between 1 and 10 μm in the simulation plan. The rate parameters chosen were shown to be valid in other work by the authors and fit within the ranges of those measured in the literature.[13–15] These distances are in the order of the particle size employed in this study.

The binary diffusion coefficient for ZnO particles in argon was assumed to be close to zero, basically amounting to the assertion that the Brownian forces leading to diffusion do not strongly affect the particles. Hinds[7] reports diffusion coefficients of micron size particles to be on the order of 1×10^{-11} m^2 s^{-1}, and for 10 nm particles this diffusion coefficient was on the order of 1×10^{-8} m^2 s^{-1}. The diffusion coefficient for the particles used in this simulation (1 μm) would then be about six orders of magnitude smaller than the gas diffusion coefficient. A value of 1×10^{-10} m^2 s^{-1} was used in the simulation.

A second energy balance was used for the "smeared out" phase of ZnO particles:

$$0 = Q_{source} + (-\nabla \cdot \rho_{ZnO,eff} C_{p,ZnO} T_{particles} \vec{v}) - (\nabla \cdot \vec{q}) \tag{23}$$

where $\rho_{ZnO,eff}$ is the effective ZnO phase density and $C_{p,ZnO}$ is the specific heat capacity of ZnO, and Q_{source} is a volumetric heat source, described below. The effective ZnO phase density was calculated by multiplying the bulk density of ZnO by the volume fraction of ZnO in the gas. As the particles were discrete, there could exist no conduction between them unless individual particles were touching, the number of which at any given time was assumed to be negligible. Therefore, the conduction term, $(\nabla \cdot \vec{q})$, was assumed to be zero. The volumetric source term, Q_{source}, could be broken into three parts:

$$Q_{source} = Q_{rad} - Q_{part} - Q_{rxn} \tag{24}$$

where Q_{rad} is the volumetric energy source term for radiation heat transfer to the particles, Q_{part} is the volumetric energy source term for conductive heat transfer between the particles and the gas, and Q_{rxn} is the volumetric energy source term for the energy required by the dissociation reaction. Heat transfer to and from the particles was assumed to only occur through radiation from the walls and other particles and through conduction to the gas phase. Additionally, thermal energy of the particle could be used to drive the endothermic chemical reaction to form oxygen and zinc vapor. The particle could lose energy through conduction to the gas phase

and by reacting to form zinc and oxygen gas. The radiation energy input was expressed by the divergence of the radiation flux:

$$Q_{\text{rad}} = -\nabla \cdot \vec{q}_{\text{r}} \tag{25}$$

The divergence of the radiation flux was calculated through solution of the transfer equation for radiative intensity:[16]

$$\frac{di'_\lambda}{dS} = -(a_\lambda + \sigma_\lambda) i'_\lambda + a_\lambda i'_{\lambda\text{b}} + \frac{\sigma_\lambda}{4\pi} \int_{\omega=0}^{4\pi} i'_\lambda \Phi(\lambda, \omega) d\omega \tag{26}$$

where i'_λ is the spectral directional radiative intensity, a_λ is the spectral absorption coefficient, σ_λ is the spectral scattering coefficient, $i'_{\lambda\text{b}}$ is the spectral blackbody intensity, ω is the unit solid angle, and $\Phi(\lambda,\omega)$ is the scattering phase function.

Mie scattering calculations were performed following Bohren and Huffman to determine the absorption and scattering coefficients of ZnO, as well as the scattering phase function.[17] The refractive index of ZnO is spectrally independent in the wavelength range of interest for radiation between 1000 and 2000 K (900 nm–8 μm), and was given by Liu et al. as:[18]

$$\bar{n} = 1.96 - 0.04i \tag{27}$$

Mie scattering calculations showed the absorption coefficient was relatively constant for the wavelength region of interest (800 nm–8 μm) for a given particle size and particle concentration, so long as particles had a diameter greater or equal to 1 μm. As a result, these were approximated as constant over all wavelengths; although not perfectly accurate, this is a good first approximation. The values of absorption coefficient ranged between 26 and 400 m^{-1}, dependent on mass loading and particle size. Scattering coefficients varied greatly with wavelength, but for all wavelengths for particles greater than 1 μm, this scattering was directed strongly forward. Thus, to simplify the solution to the problem, it was assumed that only absorption played a role, as any radiation scattered would be primarily directed in the original direction of the incident radiation. Additionally, the absorption coefficient was assumed to be independent of wavelength, temperature, and conversion. It is true that the absorption coefficient will decrease with particle size (as the particles are converted to Zn and O_2). However, as $\sim$50% of the conversion for a 1 μm particle takes place in the first 200 nm of particle size, it is safe to assume that most of the particles will be absorbing near the coefficient value for the average between a diameter of 800 and 1000 nm. The source function then becomes the intensity function for a blackbody, and the intensity transfer equation is greatly simplified:

$$\frac{di'_\lambda}{dS} = -a_\lambda i'_\lambda + a_\lambda i'_{\lambda\text{b}} \tag{28}$$

Solving this differential equation, the intensity can be found as a function of the path length S:

$$i'_\lambda = i'_\lambda(0) e^{-a_\lambda S} + \int_0^S a_\lambda i'_{\lambda\text{b}} e^{-a_\lambda (S-S')} dS' \tag{29}$$

where S is the path length from the volume element of interest to the radiating wall, S' is the path length from an attenuating volume element to the radiating wall, and $i'_\lambda(0)$ is the spectral direction intensity at the path origin (i.e. the radiating wall).

The energy delivered to a control volume in the system is then given by the integrated absorbed incident intensity over all solid angles and wavelengths:

$$Q_{\text{in,rad}} = \int_0^\infty a_\lambda \int_{\omega=0}^{4\pi} i'_\lambda d\omega d\lambda \tag{30}$$

Substituting for the integrated equation for the intensity, the integral can be split into two fractions, namely that delivered by nonattenuated radiation from the walls and that delivered by spontaneous re-emission from the surrounding particles:

$$Q_{\text{in,rad}} = \int_0^\infty a_\lambda \int_{\omega=0}^{4\pi} i'_\lambda(0) e^{-a_\lambda S} d\omega d\lambda + \int_0^\infty a_\lambda \int_{\omega=0}^{4\pi} \int_0^S a_\lambda i'_{\lambda\text{b}} e^{-a_\lambda (S-S')} dS' d\omega d\lambda \tag{31}$$

If the location of the control volume is designated by the directed vector $\vec{r}$ and the location of the source volume is designated by the directed vector $\vec{r}'$, then the path S is designated by the difference $\vec{r} - \vec{r}'$. If the tube walls are assumed black, then the equation for the energy delivered to the control volume can be expressed in cylindrical coordinates by:

$$Q_{\text{in,rad}} = a_\lambda \int_{\text{A}} \frac{\sigma_{\text{sb}}}{\pi} T_{\text{wall}}^4 \times \frac{(\vec{n} \cdot (\vec{r} - \vec{r}_0)) \exp\left(-a_\lambda \left(r^2 + r_0^2 - 2rr_0^2 \cos\varphi_0 + (z - z_0)^2\right)^{1/2}\right)}{\left(r^2 + r_0^2 - 2rr_0^2 \cos\varphi_0 + (z - z_0)^2\right)^{\frac{3}{2}}} dA + a_\lambda^2 \int_{\omega=0}^{4\pi} \int_0^S \frac{\sigma_{\text{sb}}}{\pi} T^{*4} \times \frac{\exp\left(-a_\lambda \left(r^2 + r^{*2} - 2rr^{*2} \cos\varphi^* + (z - z^*)^2\right)^{\frac{1}{2}}\right)}{\left(r^2 + r^{*2} - 2rr^{*2} \cos\varphi^* + (z - z^*)^2\right)} d\varphi^* dr^* dz^* \tag{32}$$

where the first integral is over all external surfaces, the unsubscripted coordinates refer to the location of the control volume, the coordinates subscripted with 0 refer to the points on the radiating wall, and the coordinates superscripted with * refer to points within the reactor that are emitting to the control volume. This notation is in accordance with the convention used by Siegel and Howell.[16]

The energy spontaneously emitted by the control volume is given by:

$$Q_{\text{out,rad}} = 4a_\lambda \sigma_{\text{sb}} T^4 \tag{33}$$

Thus, the net energy delivered to the particles via radiation is given by:

$$\nabla \cdot \vec{q}_r = Q_{out,rad} - Q_{in,rad} \tag{34}$$

This was directly incorporated into the partial differential equations solved by COMSOL Multiphysics, with iteratively updated numerical integration is used to solve the coupled integral equations.

The conductive heat loss to the gas was given by an integrated Fourier-type expression,[6] where the distance over which the integrated heat loss occurs is the particle radius, in accordance a Nusselt number of 2 for zero relative velocity between the particle and the surrounding gas:[19]

$$Q_{cond,gas} = \frac{2k}{D_{particle}} A_{particle} N_{particles} (T_{particles} - T) \tag{35}$$

The energy required for reaction was given by the usual relation:

$$Q_{rxn} = \Delta H_T^\circ R_{ZnO} \tag{36}$$

In addition to following the concentration of ZnO in the system, the concentration profiles of the reaction products were determined as well. The continuity equations used for the concentrations of oxygen and Zn vapor were, respectively:

$$\nabla \cdot (-D_{O_2—Ar} \nabla c_{O_2} + c_{O_2} \vec{v}) = -\frac{1}{2} R_{ZnO} \tag{37}$$

$$\nabla \cdot (D_{Zn—Ar} \nabla c_{Zn} + c_{Zn} \vec{v}) = -R_{ZnO} \tag{38}$$

where c_i is the concentration of species i and D_{i-j} is the diffusion coefficient of species i in gas j.

The diffusion coefficient of oxygen in argon was calculated using a Chapman–Enskog relation:

$$D_{O_2—Ar} = 1.8583 \times 10^{-7} \frac{\sqrt{T^3 \left(\frac{1}{M_{O_2}} + \frac{1}{M_{Ar}}\right)}}{p_{atm} \sigma_{O_2—Ar}^2 \Omega_{O_2—Ar}} \tag{39}$$

where M_i is the molecular weight for species i, σ_{O_2-Ar} is the mean characteristic diameter of oxygen and argon, and Ω_{O_2-Ar} is the diffusion collision integral for the same species. These were calculated from charts in Bird et al.[6]

Because of the lack of Lennard-Jones data available for atomic zinc vapor, experimental values for the diffusion coefficient were obtained from the literature. The diffusion coefficient of Zn vapor was found experimentally by Aref'ev, et al.[20] This value was very close to that of oxygen in the temperature ranges of interest (1400–2100 K). For this reason, the theoretically calculated value of the diffusion coefficient for oxygen was applied to Zn vapor as well.

Boundary Conditions

The geometry dimensions and assigned boundaries are shown in Figure 2. Boundary (1) is the tube centerline, boundary (2) is the center tube inlet, boundary (3) is the center tube outlet, boundary (4) is the interface between the central flow region and the porous flow region, boundaries (5) and (6) are the top and bottom of the porous flow region, respectively, boundary (7) is the interface between the porous flow region and the annular flow region, boundaries (8) and (9) are the top and bottom inlets to the annular flow region, and boundary (10) is the outer containing tube wall. The momentum, energy, and mass transfer boundary conditions are shown in Table 1.

In each of the balances, boundary (1) was assigned an axial symmetry condition, consistent with the assumption of azimuthal independence. For the momentum balance, boundary (10) was assigned a no-slip condition. This was physically consistent with a solid barrier to fluid flow. At the central flow region entrance, boundary (2); and at the annular flow entrances, boundaries (8) and (9); the z-velocity was assigned an average value based on the volumetric flow:

$$v = \frac{\dot{V}_i}{A_{cx,i}} \tag{40}$$

where $\dot{V}_i$ is the inlet volumetric flowrate at boundary i and $A_{cx,i}$ is the tube cross-sectional area at boundary i. The radial velocities were set to zero at these boundaries. At boundary (3), the central flow exit was assigned a normal flow/pressure condition:

$$\vec{t} \cdot \vec{v} = 0 \tag{41}$$

$$\vec{n} \cdot \left[-p + \mu(\nabla \vec{v} + (\nabla \vec{v})^T) - \frac{2}{3}\mu(\nabla \cdot \vec{v})\right] \vec{n} = -p_0 \tag{42}$$

where $\vec{t}$ is a unit vector tangential to the boundary and $\vec{n}$ is a unit vector normal to the boundary. The pressure p_0 was set to 1 atm. The top and bottom of the porous region, boundaries (5) and (6), respectively, were assigned no-slip conditions. The porous tube would be expected to be fitted to a solid piece, preventing any gas flow through the joint.

The interfaces between the porous flow region and the central and annular flow regions had two-sided boundary conditions. For the interface between the annular and porous regions, boundary (7), the momentum balance boundary condition on the annular region side was set to an outflow/pressure condition:

$$p = p_0 \tag{43}$$

with p_0 set to the pressure on the boundary solved for in the porous region. On the porous side of the boundary, the r- and z-velocities were set equal to those on the boundary solved for in the annular flow region. This combination of Dirichlet and Neumann boundary conditions ensured solution continuity across the boundary. Likewise, at the interface between the porous and central flow regions, the momentum boundary condition on the porous side was set to a similar outflow/pressure condition, with the pressure set to that solved for on the boundary in the central flow region. The velocities on the boundary in the central flow region were set to those solved for on the boundary for the porous region.

In the energy balance, boundary conditions had to be specified for both the gas and particle phases. For boundary (2), the inlet temperature of the gas and particles was set to room temperature, 298 K. At boundary (3), a "convective flux" condition was employed:

$$\vec{q} \cdot \vec{n} = \rho C_p T \vec{v} \cdot \vec{n} \tag{44}$$

Table 1. Boundary Conditions

Boundary	Momentum	Energy		Mass		
		Gas	Particles	ZnO	Zn	O_2
1	Axial symmetry	Axial symmetry	Axial symmetry	Axial symmetry	Axial symmetry	Axial symmetry
2	$v_z = \frac{\dot{V}_{\text{central}}}{A_{\text{cx,central}}}$ $v_r = 0$	$T = 298$ K	$T_{\text{part}} = 298$ K	$c_0 = \frac{\dot{m}_{\text{ZnO}}}{M_{\text{ZnO}}\dot{V}_{\text{gas}}}$	$c_0 = 0$	$c_0 = 0$
3	Normal flow/$p = 0.1$ MPa	Conv. flux	Conv. flux	Conv. flux	Conv. flux	Conv. flux
4	Central side: $\vec{v}_{\text{central}} = \vec{v}_{\text{porous}}$ Porous side: Outflow/$p_{\text{porous}} = p_{\text{central}}$	Central side: $T_{\text{central}} = T_{\text{porous}}$ Porous side: Conv. flux	$\vec{q} = 0$	$\vec{N}_{\text{ZnO}} = 0$	$\vec{N}_{\text{Zn}} = 0$	$\vec{N}_{\text{O}_2} = 0$
5	No slip	$\vec{q} = 0$	N/A	N/A	N/A	N/A
6	No slip	$\vec{q} = 0$	N/A	N/A	N/A	N/A
7	Porous side: $\vec{v}_{\text{porous}} = \vec{v}_{\text{annular}}$ Annular side: Outflow/$p_{\text{annular}} = p_{\text{porous}}$	Porous side: $T_{\text{porous}} = T_{\text{annular}}$ Annular side: Conv. flux	N/A	N/A	N/A	N/A
8	$v_z = \frac{\dot{V}_{\text{top}}}{A_{\text{cx,ann}}} v_r = 0$	$T = 298$ K	N/A	N/A	N/A	N/A
9	$v_z = \frac{\dot{V}_{\text{bottom}}}{A_{\text{cx,ann}}}$ $v_r = 0$	$T = 298$ K	N/A	N/A	N/A	N/A
10	No slip	$T = T_{\text{wall}}$	N/A	N/A	N/A	N/A

This specifies a boundary flux equal to the enthalpy of the material leaving the reactor and was used for both the gas and particle phases. The only remaining boundary condition for the particles was at the central flow region/porous region interface, as the particles were not permitted to pass through the porous region. This was set to thermal insulation. The particles could not be thought to be, in general, in contact with the porous wall, and so there would be no appreciable particle-porous medium conductive energy transport. The annular entrances (boundaries (8) and (9)) were assigned room temperature (298 K) Dirichlet conditions for the gas phase, similar to that of boundary (2). The top and bottom of the porous region, boundaries (5) and (6), respectively, were assigned thermal insulation conditions. The gas could not convectively carry energy across those boundaries, and conductive heat transfer from the gas to the support for the porous material was assumed to be negligible compared with any conductive heat transfer from the porous medium itself to its support. The outer wall of the annular region, boundary (10), was set to a specified wall temperature between 1900 and 2200 K. Because of the laminar nature of the gas flow near the wall in the annular region ($Re \sim 10$), radial transfer of energy from the wall was assumed to occur only by conduction, and a local temperature of the gas equal to the wall temperature was appropriate.

At the interfaces between the porous region and the free flow region, the boundary conditions were again two-sided. On the annular flow region side of boundary (7), the gas was given a convective flux condition. On the porous flow side of the same boundary, the gas temperature was set to the temperature solved for on the boundary in the annular flow region. Similarly, on the porous flow side of boundary (4), the gas was given a convective flux condition, and on the central flow side of the same boundary, the gas temperature was set equal to the temperature solved for on the porous flow side of that boundary.

The mass transfer boundary conditions were as follows: at boundary (2), the central flow entrance, the concentration of ZnO was defined by the inlet ZnO flowrate and the inlet gas flowrate:

$$c_0 = \frac{\dot{m}_{\text{ZnO}}}{M_{\text{ZnO}}\dot{V}_{\text{gas}}} \tag{45}$$

The concentrations of O_2 and Zn(g) were set to zero at this boundary, as they could only appear by dissociation of ZnO. At boundary (3), a convective flux condition similar to that in the energy equations was used for all species:

$$\vec{N}_i \cdot \vec{n} = c_i \vec{v} \cdot \vec{n} \tag{46}$$

where $\vec{N}_i$ is the molar flux of species i. At boundary (4), the flux of ZnO was set equal to zero. This corresponds to an assumption that ZnO particles were too large to pass through the pores of the permeable material. The flux of Zn at the surface was similarly set equal to zero. For the oxygen balance, the concentration of O_2 at the boundary was set equal to zero. The porous wall was assumed to be constructed of some oxidation sensitive material. At elevated temperatures, the surface reaction rate of oxygen with such a material was assumed to be very large, and the controlling kinetic factor was assumed to be oxygen transport to the wall. Therefore, oxygen reaching the wall was assumed to be instantly consumed by reaction, and a zero concentration of O_2 at the wall was used.

Experimental Apparatus

Experiments were conducted at the High Flux Solar Furnace (HFSF) facility, part of the National Renewable Energy Laboratory located in Golden, CO. These were designed to determine the effectiveness of a fluid wall for prevention of

reaction of oxygen with a graphite reactor tube. The HFSF used an off-axis heliostat-primary concentrator arrangement to deliver an approximately 0.1 m^2 concentrated solar energy beam to the secondary concentrator. The secondary concentrator further concentrated this energy by a factor of ~2, and a back reflector was wrapped around the reactor to provide solar heating evenly around the tube. A pyrometer was used to measure the temperature of the reactor tube.

The reactor configuration employed is shown in Figure 3. It consisted of three concentric tubes. The outer tube was 0.0508 m in inner diameter and consisted of quartz. This tube provided a window to enclose the oxidation sensitive outer tubes. The "middle" tube had an inner diameter of 0.021 m and was constructed of solid glassy carbon. Finally, the "inner" tube was 0.012 m in inner diameter and was constructed of porous graphite. Solid ZnO particles were introduced into the "inner" tube by a spinning wheel feeder/vibrating tray apparatus. The vibrating tray shook the particles onto the rotating titanium wheel, which was designed to shear and disperse large agglomerates of particles. At this point, the particles were entrained in argon gas flow to move them down into the "inner" tube.[21]

Argon gas was introduced at the top and the bottom of the annular region between the "inner" and "middle" tubes. A pressure drop across the porous graphite "inner" tube would result, forcing the argon gas radially into the central flow region, as described in the fluid wall concept above. The top and bottom annular gas flows were controlled independently with MKS mass flow controllers. In the annular space between the "outer" quartz tube and the "middle" solid carbon tube, argon gas was flowed upward to keep the quartz below an acceptable maximum operating temperature (<400°C).

Upon leaving the "inner" tube, the reaction products and unreacted particles were quenched in a 1.91 cm diameter water-cooled stainless steel tube. Heavy particles were collected by gravity in a collection vessel, whereas lighter, entrained particles were collected in an HEPA filter downstream of the collection vessel. Gas flow was measured using an OMEGA thermal mass flow meter, as well as a Sponsler turbine-style volumetric flow meter. Gases were analyzed for O_2 using an AMI electrochemical Series 201 oxygen analyzer, and for CO and CO_2 using a California Analytical Instruments Model 602 nondispersive infrared gas analyzer. A LECO TC-600 combustion oxygen analyzer was used to measure the oxygen content by mass of the collected samples, and conversion could be calculated from this measurement. Calculation of the sample conversion could then be made from the measurement:

$$X_{\mathrm{ZnO}} = \frac{\frac{1}{M_{\mathrm{Zn}}}\left[m_{\mathrm{sample}} - (m_{\mathrm{sample}} c_{Ox}) - \left(\frac{M_{\mathrm{Zn}}}{M_{\mathrm{O}}} m_{\mathrm{sample}} c_{Ox}\right)\right]}{\frac{1}{M_{\mathrm{Zn}}}\left[m_{\mathrm{sample}} - (m_{\mathrm{sample}} c_{Ox}) - \left(\frac{M_{\mathrm{Zn}}}{M_{\mathrm{O}}} m_{\mathrm{sample}} c_{Ox}\right)\right] + \frac{m_{\mathrm{sample}}}{M_{\mathrm{O}}} c_{Ox}} \tag{47}$$

where M_i is the molecular weight of species i, m_{sample} is the mass of the collected sample, and c_{Ox} is the mass fraction of oxygen in the sample as measured by the LECO TC600.

A $2^{4-1}{}_{\mathrm{IV}}$ fractional factorial experimental design with two center points was used to test for the effectiveness of the fluid wall at prevention of reaction. This design is shown in Table 2.

Results and Discussion

Mesh studies

The mesh used in the simulations consisted of triangular elements. The resolution of the mesh was about twice as dense in the thin annular and porous regions as it was in the central region. Cases of increasing mesh resolution were performed at a variety of representative flow and wall temperature conditions to determine the sufficient mesh resolution for solution stability. The number of mesh elements increased by ~10% between each case. The metrics used for determining solution stability were the outlet boundary integrals of ZnO and O_2 flux, the integral over the boundary between the porous and central flow regions of the radial velocity, and the temperature integral over the entire reactor volume. For 37,640 mesh elements and 333,741 degrees of freedom, all of the measurements were within 1% of the next highest mesh resolution. At this mesh resolution, the nodes are an average distance of 0.5 mm from each other in the central region and at an average distance of 0.23 mm from each other in the annular and porous regions. This was deemed sufficient. It was this resolution that was used in the simulations discussed below.

General results

Surface plots of a representative converged simulation are shown in Figures 4a–e. In the figures, the leftmost boundary is the centerline of the simulated space. As shown in Figure 2, the leftmost rectangle represents the center region, the center rectangle represents the porous region, and the rightmost rectangle represents the annular region. From Figure 4a, the flow showed laminar characteristics in the central and annular regions. Reynolds numbers ranged between 1 and 15. The gas velocity increased down the reactor because of the addition of the gas passing through the porous region from the annular region to the central gas flow. For this reason, residence times in the reactor depended both on total gas flow volume and distribution of that flow across the porous region.

The gas and particle temperatures are shown in Figures 4b, c, respectively. The particle temperature is only plotted in the central region since the boundary conditions did not allow particles to enter the porous region. Examining the general temperature trends, it could be seen that gas and particles alike in the central flow region heated up nearly instan-

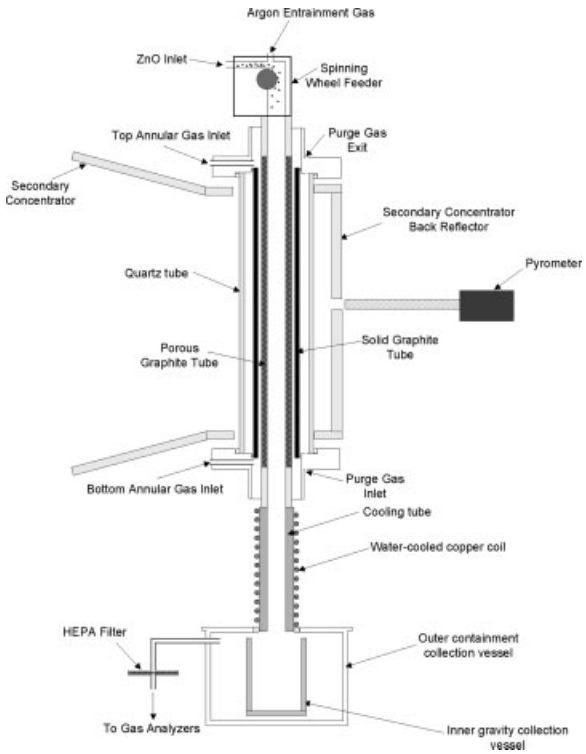

Figure 3. Experimental apparatus for on-sun ZnO dissociation at NREL.

taneously. The absorption of radiation by the particles is evidently very strong as they heat up rapidly upon entrance into the reactor. This particle temperature is fairly uniform, a result of particle-to-particle radiation. Evidently, the particle loading used in these simulations is not high enough to see significant "shielding," where particles near the wall prevent those in the center from receiving the wall radiation. This shielding is a function of thermal mass; here the thermal mass is not high enough near the wall to introduce significant heating lag or temperature gradients across the reactor. In larger diameter systems, this could be an issue, but this factor is not central to the goals of this study. The instantaneous particle heating allows one to assume the particle temperature as the wall temperature at all points in the reactor when designing such a system. The gas temperature profile was nearly identical to that of the particles. The high surface area

Table 2. Fractional Factorial Design for NREL Fluid Wall Reactor Experiments

Run Order	Central Flow (SLPM)	Wall Temperature, K	Top Annular Flow (SLPM)	Bottom Annular Flow (SLPM)
7	1	2000	0.66	1.33
2	3	2000	1.33	0.66
8	1	2300	2	1
3	3	2300	1	2
10	1	2000	1.33	0.66
5	3	2000	0.66	1.33
4	1	2300	1	2
9	3	2300	2	1
6	2	2150	1.25	1.25
1	2	2150	1.25	1.25

to volume ratio of the particles allows for rapid heat exchange between the phases. This validates the concept of using particles as radiation heat transfer agents to the gas, suggested elsewhere in the literature.[2] In the annular region, the gas heated quickly as well, a result of short conduction distances, and temperature in the porous region was very close to the wall temperature. This was largely because of the heating of the gas as it passed through the interstices of the porous tube; the effects of adjustments to this heating rate are described below.

The most interesting effects could be seen in the concentration surface plots, Figures 4d, e. As these values were only defined in the central region, the areas of the plot representing the porous and annular regions were left blank. In Figure 4d, the concentration profile for ZnO is shown. The concentration dropped rapidly as the gas heated up, resulting from a drop in gas and particle phase density. As the particles moved down the tube, a boundary layer developed close to the porous wall. Concentration of ZnO inside the boundary layer was essentially zero. A concentration gradient of nearly 1 mol/m^3 appeared across the boundary layer, caused by the radial influx of gas from the porous region. Because of the low diffusion coefficient assigned to the particles, they did not move against the effusive radial flow from the porous region with any appreciable velocity, and they were effectively segregated from the wall. This appears very promising for the use of a fluid wall as an oxidation protection device. If the particles were kept away from the wall by the radial effusive flow, there is hope that oxygen would be as well.

Examining the oxygen concentration in the system (Figure 4e), this appeared to be, in some sense, the case. The oxygen concentrations were very high in the central portion of the tube, and they were low near the porous wall. However, it must be recalled that as oxygen was assumed to react away instantly at the boundary, the concentration should be low there. A better measure for the protective ability of the fluid

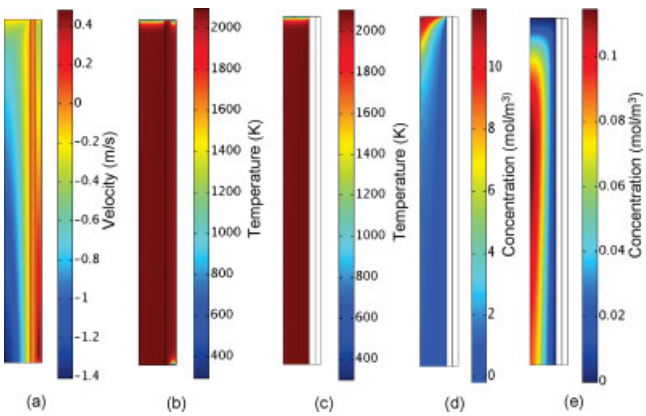

Figure 4. Surface plots for a representative converged simulation of (a) *z*-velocity, (b) gas temperature, (c) particle temperature, (d) ZnO particle concentration, and (e) O_2 concentration (T_{wall} = 2000 K, $V_{central}$ = 1.0 SLPM, V_{top} = 0.75 SLPM, V_{bottom} = 0.75 SLPM).

[Color figure can be viewed in the online issue, which is available at www.interscience.wiley.com.]

wall is the conversion of O_2 produced by the dissociation of ZnO to CO_2. This is discussed in further detail below.

Conversion studies and fluid-wall effectiveness

The desired effect of these aerosol reactors is to maximize conversion of ZnO with minimal corrosive oxidation of the tube wall. Conversion of ZnO at axial planes in the reactor was calculated by integrating the flux across the planal boundaries:

$$X_{\mathrm{ZnO}} = 1 - \frac{\dot{n}_{\mathrm{ZnO,out}}}{\dot{n}_{\mathrm{ZnO,in}}} \tag{48}$$

where $\dot{n}_{\mathrm{ZnO,in}}$ is the molar flowrate of ZnO entering the reactor and $\dot{n}_{\mathrm{ZnO,out}}$ is the molar flowrate of ZnO leaving the reactor. The effect of wall temperature and central gas flow on fractional conversion of ZnO for an even annular gas flow distribution is shown in Figure 5. Conversion increased nearly exponentially with temperature, in agreement with the Arrhenius rate law. As would be expected, the conversion increased as the central gas flow decreased. This would increase the residence time, and it makes perfect sense that conversion would increase as residence time in the reactor increased. Average conversions greater than 50% could be achieved by operating the reactor above 2050 K and with central inlet gas flow rates less than 1.0 SLPM. The maximum conversion observed in the reactors was for a wall temperature of 2200 K and a central gas flowrate of 0.5 SLPM, and this conversion was 92%. Figure 6 shows the analogous plot for variation of annular gas flow distribution, with a constant wall temperature of 2100 K and a central flowrate of 1.0 SLPM. Again, for residence time reasons, higher total gas flowrates resulted in lower exit conversions of ZnO. The distribution of gas across the annular gas inlets did not appear to be important, reflecting a fairly even gas distribution through the porous wall regardless of where flow entered the annular region.

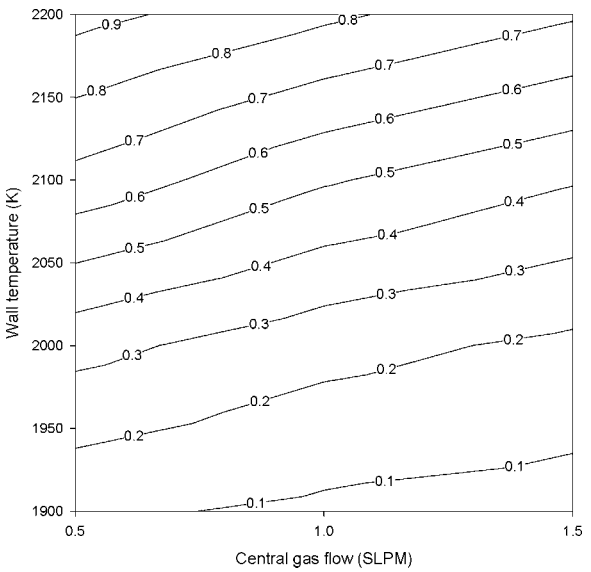

Figure 5. Effect of wall temperature and central gas flow on fractional conversion of ZnO (V_{top} = 0.75 SLPM, V_{bottom} = 0.75 SLPM).

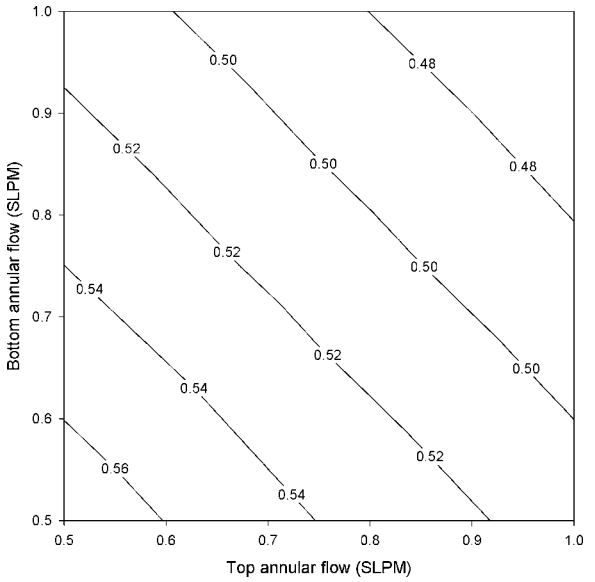

Figure 6. Effect of annular gas flow distribution on exit ZnO conversion (T_{wall} = 2100 K, V_{central} = 1.0 SLPM).

It was desired to know the axial distribution of radial gas flow through the porous wall, as this was expected to be a determining factor in the effectiveness of the fluid wall at preventing oxidation of the reactor. Figure 7 shows the radial gas velocity at the exit of the porous section as a function of axial distance for four different wall temperatures and a constant permeability of 1×10^{-11} m^2, and Figure 8 shows the analogous plot for four different values of the porous wall permeability and a constant wall temperature of 2100 K. From Figure 7, it can be seen that radial velocity distribution was not strongly affected by the gas temperature, but the absolute values of the velocity increased with temperature.

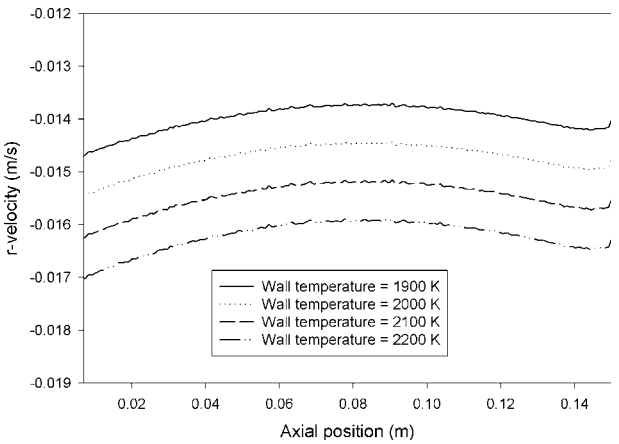

Figure 7. Axial profile of radial gas velocity at the exit of the porous section for varying wall temperature.

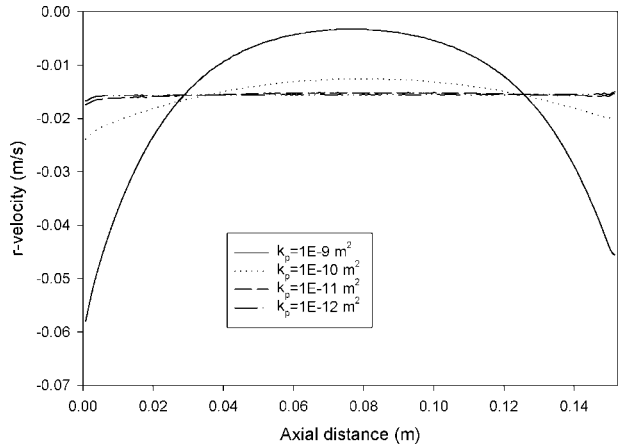

Figure 8. Axial profile of radial gas velocity at the exit of the porous section for varying porous medium permeability.

This was a result of the decrease in density of the gas as temperature increased, but the increase in gas velocities did not necessarily mean an improvement in the ability of the fluid wall to prevent oxidation. As gas temperature increases, the diffusion coefficient of oxygen increases with it, and the increased radial velocity of the inert gas may be offset by increased diffusive velocity of oxygen in the opposite direction. The effectiveness will be explored below, when oxygen concentrations in the gas are considered.

When the permeability was varied, large changes in the gas flow were observed. At the highest value of the permeability examined (1×10^{-9} m^2), most of the gas entered the central region at the very top and bottom of the porous tube. As the permeability decreased, the distribution of radial gas velocity through the porous tube became more even. As the permeability decreased, the required pressure drop for a given gas velocity also increased. This allowed greater pressure to build across the annular flow region, and in the simulations this caused the flow to be more evenly distributed.

Even distribution of flow would be seen as a desirable design goal. Because oxygen must diffuse to the wall in order to react with it, regions with less inward radial inert gas flow would be more vulnerable to oxidative corrosion. If any asymmetry were desired, it would be to have slightly higher flows in the lower portion of the reactor, where oxygen concentrations were higher (because of cumulative conversion of ZnO). However, this asymmetry could be controlled by controlling the inlet gas flowrates at the top and bottom of the annular section, and would be easier to control if the permeability of the porous region was not influencing the gas distribution. Therefore, a material with a low value ($<1 \times 10^{-11}$ m^2) of permeability should be selected.

This assertion about protective ability needed to be tested, though. The effectiveness of the fluid wall at preventing oxidation is examined in Figures 9 and 10. The conversion of product oxygen to CO_2 was calculated by comparing the flux of CO_2 with the conversion of ZnO:

$$X_{CO_2} = \left[1 - \frac{2\dot{n}_{CO_2,out}}{X_{ZnO}\dot{n}_{ZnO,in}}\right] \quad (49)$$

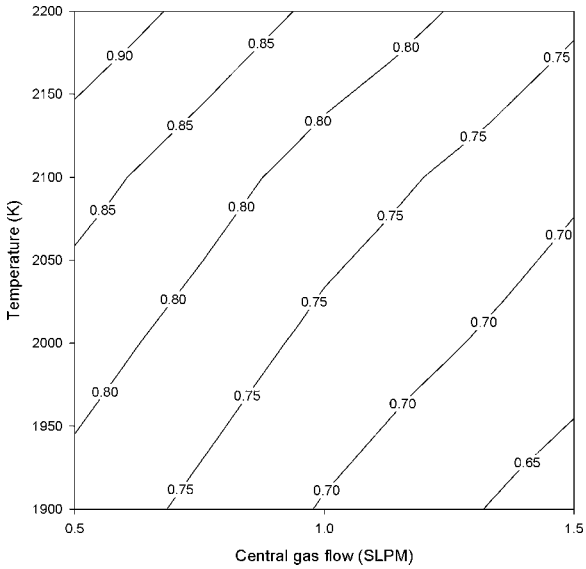

Figure 9. Dependence of corrosive O_2 conversion at reactor wall on wall temperature and central gas flow (V_{top} = 0.75 SLPM, V_{bottom} = 0.75 SLPM).

where $\dot{n}_{CO_2,out}$ is the molar flowrate of CO_2 out of the system. In Figure 9, conversion of oxygen that was generated by dissociation of ZnO is shown as a function of wall temperature and central gas flow for an even fluid wall distribution, with 0.75 SLPM entering both annular inlets. These simulations were conducted for a material permeability of 1×10^{-11} m^2. As the wall temperature was increased, the degree of reaction of oxygen with the wall also increased. This would be expected, as the diffusion coefficient of oxygen increases with temperature. Likewise, as the central flow was decreased, the conversion of oxygen also decreased, as the

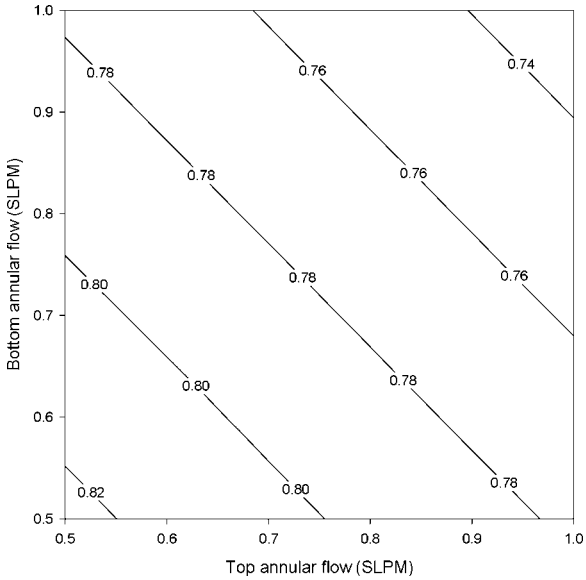

Figure 10. Dependence of corrosive O_2 conversion at reactor wall on annular gas flow distribution (T_{wall} = 2100 K, $V_{central}$ = 1.0 SLPM).

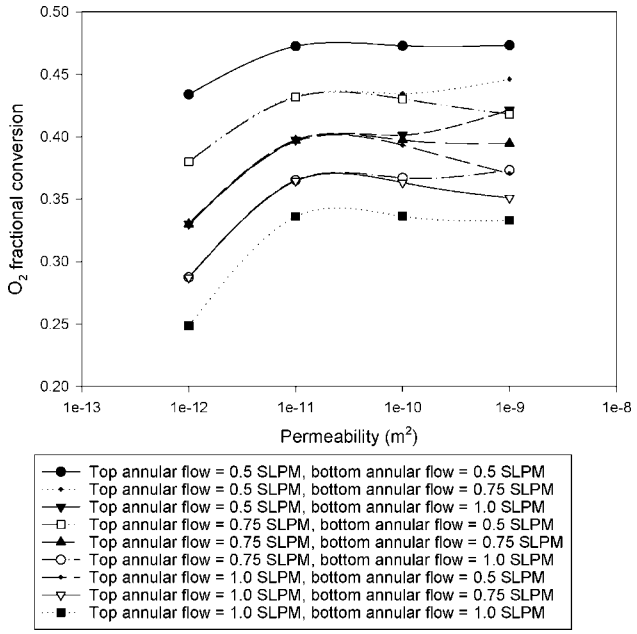

Figure 11. Effect of varying porous material permeability on corrosive conversion of O_2 at reactor wall.

concentration gradient driving force for diffusion would be reduced. To minimize oxidation, one would operate the reactor at a low wall temperature and a high central inlet gas flow rate.

Figure 10 shows the analogous plot for oxygen conversion as a function of inlet gas flow distribution in the annular region. These studies were performed for a wall temperature of 2100 K and a central gas flow of 1.0 SLPM. Again, higher total gas flow rates lead to lower corrosive conversion of oxygen. As the gas flow was increased, the effusive barrier of radial gas flow to diffusion of oxygen became stronger, and the overall oxygen conversion dropped. Again, one would operate the reactor at high annular gas flowrates to minimize corrosive oxidation of the reactor wall.

Above, the operating conditions for minimal oxygen conversion were highlighted: low wall temperature combined with high central and annular gas flowrates. However, these are exactly the opposite of the recommended conditions for high ZnO conversion! If a fluid wall were to be employed to limit oxidation, making it most effective would severely limit the reactor's ability to do its job, which is converting ZnO to Zn and O_2. More important, though, is the magnitude of the oxygen conversions. In each case, they exceeded 60% of that generated. For a ZnO inlet flowrate of 1 g/min, with ZnO conversion of 60% and subsequent conversion of 60% of the generated oxygen, a graphite tube would oxidize at the rate of 0.053 g/min. For a tube diameter of 2.29 cm, a length of 15.24 cm, a thickness of 0.254 cm, and a graphite density of 2267 kg/m^3, the tube would oxidize away completely in under 10 h. This would be expected to scale with reactor size (as ZnO flowrate would scale with size) and represents an unacceptable and impractical rate of reactor corrosion. Such a reactor could not be employed in a commercial solar plant.

It was stated above that a better distribution through the fluid wall should reduce reaction of oxygen. This is proven in Figure 11, which shows the conversion of oxygen as a function of permeability for a variety of annular gas distributions. At lower values of permeability, when gas distribution was seen to be more even, conversion of O_2 was indeed lower. Conversion also decreased with increased gas flow, as was shown in Figures 9 and 10. At a given total annular flow, there was little difference in oxygen conversion based on distribution at low values of permeability. At high values of permeability, though, some splitting was seen for different gas distributions. When more gas entered at the top of the reactor than in the bottom, conversion of O_2 decreased, reflecting the fact that even though radial flow was not evenly distributed, the additional gas at the top of the reactor resulted in a lower diffusion rate for oxygen. In the opposite case, when flow in the bottom inlet was higher than in the top inlet, the conversion of O_2 increased. When most of the radial flow was at the ends of the reactor (i.e. high permeability), the gas entering the bottom of the reactor would simply exit immediately. Thus, for higher bottom annular inlet flowrates and poor gas distribution, a larger portion of the "protecting" fluid wall was wasted by immediately exiting the reactor, and the system showed higher levels of oxidation. Still, the levels of oxidation were high, no matter what case was examined, and these were simply too great for practical implementation.

One of the key assumptions in the model dealt with heating of the gas as it passed through the porous region. This heat transfer was modeled as if the porous region were a packed bed of particles, and the heat transfer rate to the gas depended on the size of particles chosen for this packed bed model. In the base case, a particle size of 1 mm was chosen; increasing this size would decrease effective heat transfer, and vice versa. Because the heat transfer to the gas through the porous region brought the gas nearly to the wall temperature for the 1 mm particle size (seen in Figure 4b), making the particles any smaller would not yield much different results. Instead, the effect of increasing the particle size was explored by multiplying the porous region volumetric heat source term, Q_{porous}, by a scaling factor ranging between 0.1 and 0.001. The results of this study are shown in Figure 12,

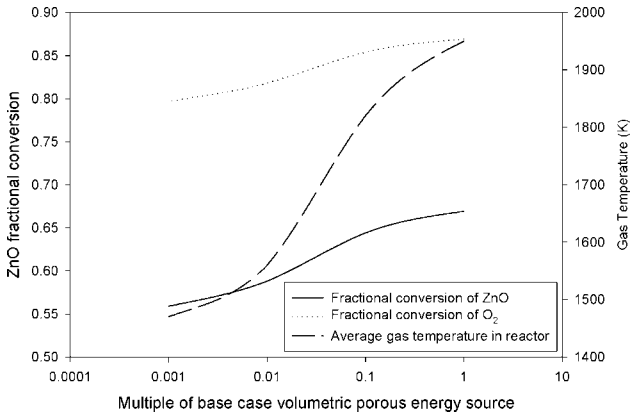

Figure 12. Effect of diminishing heat transfer to gas in porous region on exit conversion of ZnO and average gas temperature.

with the simulation performed for a wall temperature of 2100 K, a central flow of 0.5 SLPM, annular flows of 0.75 SLPM, and a permeability of 1×10^{-11} m^2. The gas temperature was greatly affected, as Q_{porous} varied over three orders of magnitude. However, this affected the conversions only slightly—about 10% magnitude adjustment for ZnO, and about a 5% magnitude adjustment for O_2 conversion. As the lowest value of Q_{porous} equated to treating the packed bed as consisting of 1-m-diameter spheres (a ridiculously large size for such a model), there was no reason to look at even smaller values of Q_{porous}. With only small changes in the overall conversions of the two species of interest, the differences in heating effects of the gas as it passed through the porous wall had little effect on the conclusions drawn from the simulations.

Experimental results

The conclusion that the fluid wall concept is not effective for preventing gas diffusion, but could be effective for keeping particles away from a wall, has been borne out by experiment. A sample trace from the ZnO dissociation experiments performed in the graphite fluid wall reactor at NREL is shown in Figure 13. In this experiment, as in all of the experiments performed at NREL, any reaction product observed in the gas phase was in the form of carbon oxides (CO and CO_2). No oxygen products were observed, indicating that all oxygen formed by thermal dissociation of ZnO reacted with the tube wall. Figure 14 shows the effect of outer wall temperature on overall conversion of ZnO in the fluid wall reactor for the experimental points in Table 2. Error bars were calculated from the standard deviation of multiple measurements on identical samples in the LECO TC-600 combustion oxygen analyzer. Because of feeding limitations, gas flowrates were relatively high compared to those examined in the simulations. As a result, conversions were relatively low, and the experimental uncertainty in the residence times removes the ability to statistically determine a residence time effect. Clearly, there was an effect, as conversions for two different flow conditions (those at 1700°C)

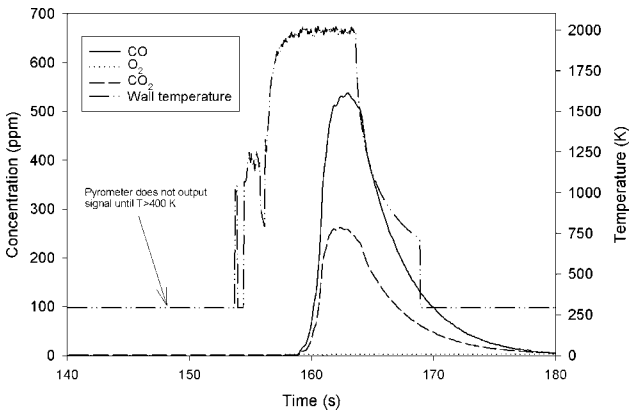

Figure 13. Product gas analysis for a representative on-sun ZnO dissociation experiment at NREL (T_{wall} = 2000 K, V_{central} = 1.0 SLPM, V_{top} = 1.33 SLPM, V_{bottom} = 0.66 SLPM, 1 g/min ZnO feed rate).

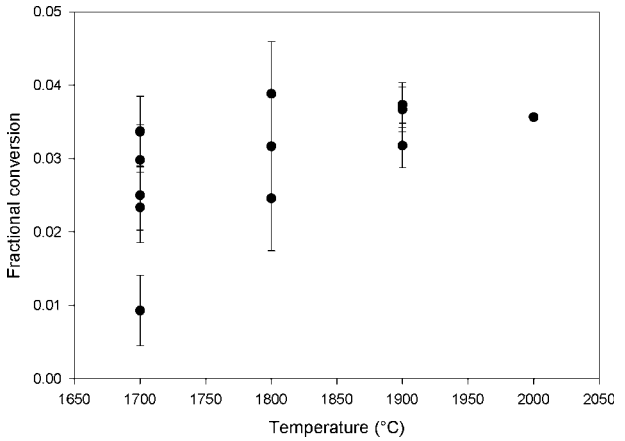

Figure 14. Effect of temperature on overall conversion of ZnO in an on-sun fluid wall reactor.

showed different overall conversions, but the statistical uncertainty disallowed a trend to be drawn with residence time over all of the experiments. Conversion increased with temperature, as would be expected, and the conversions were similar to those that could be extrapolated from the simulations for these short residence times. For the given level of conversion and the mass feed rates used, between 20 and 160 mg of Zn was produced in each experiment. Even at these very low levels of conversion, the fluid wall could not prevent the reaction of oxygen with the tube wall, and would be seen as an ineffective strategy for prevention of oxidative corrosion at high temperatures. On a final note, one of the experiments, at 1800°C, had a large degree of uncertainty in the measured conversion values. This was because of a heterogeneous nature of the collected powder. Although most of the powder was fine dust, some was fused and of higher oxygen content; this material likely sintered during feeding and was unreacted, whereas the finer material experienced reduced mass and heat transfer resistance and saw some conversion. This was the only experiment with very wide variability.

However, experimental work performed by Dahl et al. in an identical system for the dissociation of methane showed the prevention of carbon black particle buildup on the reactor walls.[2,22] In that work, there was no evidence of reactor wall corrosion or reactor wall erosion, and little buildup of particles on the wall was seen. This confirmed the idea that the fluid wall can be an effective barrier for particles with low diffusion coefficients.

Conclusions

Simulations of a high temperature fluid wall reactor for ZnO dissociation showed rapid heat transfer to both gas and particles. The gas and particles were shown to heat nearly instantaneously, a result of the massive amount of radiation heat transfer from the wall and efficient heat transfer to the gas from the particles. Because of this, when choosing operating conditions for such a reactor, the designer should assume the reacting particles to be uniformly at the wall temperature.

Distribution of gas through the porous region was not a function of temperature, but depended strongly on permeability. High permeability allowed most of the gas in the annular region to pass through the porous region near the bottom and top of the reactor. Lower permeability gave a more even distribution of radial gas velocity, and this resulted in lower overall oxidation of the porous wall.

Conversion of ZnO increased exponentially with temperature and decreased as gas was added, whether in the annular region or in the central region. Distribution of gas between the annular inlets had no effect on the outlet conversion. It was concluded that to maximize conversion, one would operate the system at as high a temperature and as low a flowrate as was reasonable.

Oxygen conversions followed a similar trend, increasing with temperature and decreasing with flowrate. However, as conversion of oxygen was undesirable, the recommended operating conditions would be opposite of those for maximizing Zn yield. The dilemma was relieved by the fact that, in all cases, oxygen conversion magnitudes were unacceptably large. Any chemical reactor constructed for ZnO dissociation with such a porous wall would quickly corrode away.

Experiments showed that, although oxygen conversion in a fluid wall reactor was unacceptably high, the fluid wall strategy could work for keeping particles away from a reactor wall. This was highlighted in the simulations, where a boundary layer containing essentially no ZnO particles developed at the edge of the porous wall. Such a boundary layer did not exist for oxygen. Fluid wall reactors are effective concepts for containing and controlling particle flow, but do not work to prevent rapid high temperature gas–surface reactions with a reactor wall. When designing such a reactor, oxidation resistant materials must to be employed.

Acknowledgments

The authors would like to acknowledge the National Science Foundation for its support through the Graduate Research Fellowship program, the Department of Education Graduate Assistanceship in Areas of National Need (GAANN) program for financial support, and the US Department of Energy for its support under grant No. DE-FG36-03GO13062.

Notation

$A_{cx,i}$ = Cross sectional area at boundary i, m^2
$A_{particle}$ = Surface area of a single particle, m^2
$A_{part,vol}$ = Surface area to volume ratio of the particles in the packed bed model for the porous region, m^{-1}
A_{porous} = Outer lateral surface area of porous tube, m^2
a_λ = Absorption coefficient, m^{-1}
C_p = Heat capacity of argon, J kg^{-1} K^{-1}
$C_{p,gas}$ = Molar heat capacity of argon, J mol^{-1} K^{-1}
$C_{p,part}$ = Molar heat capacity of particle phase, J mol^{-1} K^{-1}
$C_{p,ZnO}$ = Heat capacity of ZnO, J kg^{-1} K^{-1}
c_i = Concentration of species i, mol m^{-3}
$c_{i,0}$ = Inlet concentration of species i, mol m^{-3}
c_{Ox} = Mass fraction of oxygen in experimentally collected sample
D_{i-j} = Diffusion coefficient of species i in medium j, m^2 s^{-1}
$D_{particle}$ = Diameter of ZnO particles, m
$D_{part,porous}$ = Diameter of particles used to model porous region, m
E_a = Activation energy in Arrhenius kinetic model, J mol^{-1}
$\vec{g}$ = Gravitational force vector, N
h_{porous} = Film heat transfer coefficient in the porous section, W m^{-2} K^{-1}
I = Identity matrix
i'_λ = Spectral directional radiative intensity, W m^{-3} steradian^{-1}
$i'_{\lambda b}$ = Spectral directional radiative intensity of a blackbody, W m^{-3} steradian^{-1}
k = Thermal conductivity of argon, W m^{-1} K^{-1}
k_0 = Pre-exponential factor in Arrhenius kinetic model, s^{-1}
k_p = Permeability of porous material, m^2
k_{porous} = Thermal conductivity of the porous region, W m^{-1} K^{-1}
L = Length of tubular reactor, m
M_i = Molecular weight of species i, g mol^{-1}
m_{sample} = Mass of experimentally collected sampled, kg
$\dot{m}_{ZnO}$ = Mass feed rate of ZnO, kg s^{-1}
N_A = Avogadro's number
$N_{particles}$ = Number of particles per unit volume, m^{-3}
$\vec{N}_i$ = Molar flux of species i, mol m^{-2} s^{-1}
$\vec{n}$ = Unit vector normal to boundary
$\bar{n}$ = ZnO complex refractive index
$\dot{n}_{gas}$ = Molar flowrate of gas, mol s^{-1}
$\dot{n}_{ZnO,in}$ = Molar flowrate of ZnO into system, mol s^{-1}
$\dot{n}_{ZnO,out}$ = Molar flowrate of ZnO out of system, mol s^{-1}
$\dot{n}_{CO_2,out}$ = Molar flowrate of CO_2 out of system, mol s^{-1}
p = Gas pressure, N m^{-2}
Pr = Prandtl number for the gas in the porous region
$Q_{gas,tot}$ = Power required to heat gas to wall temperature, W
$Q_{in,rad}$ = Volumetric source term for radiation absorbed by control volume, W m^{-3}
$Q_{out,rad}$ = Volumetric source term for radiation emitted by control volume, W m^{-3}
Q_{part} = Volumetric source term for conduction heat transfer from particles to gas, W m^{-3}
$Q_{part,tot}$ = Power required to heat ZnO particle phase and dissociate the ZnO, W
Q_{porous} = Volumetric source term for energy transport from porous material to gas, W m^{-3}
Q_{rad} = Volumetric source term for radiation energy transport from wall to particles, W m^{-3}
$Q_{rad,in}$ = Power received by the porous section due to radiation, W
Q_{rxn} = Volumetric source term for energy required to dissociation ZnO, W m^{-3}
Q_{source} = Volumetric source term for energy equation, W m^{-3}
q = Number of atoms of Zn per unit surface area of solid, m^{-2}
$\vec{q}$ = Conductive heat flux, W m^{-2}
$\vec{q}_r$ = Radiative flux, W m^{-2}
R = Ideal gas constant, N $mmol^{-1}$ K^{-1}
Re_p = Particle Reynolds number in packed bed model of porous region
R_{ZnO} = Volumetric dissociation rate of ZnO, mol m^{-3} s^{-1}
$\vec{r}$ = Vector from origin to control volume
$\vec{r}_0$ = Vector from origin to point on system boundary
r_0 = Radial coordinate of point on system boundary
r^* = Radial coordinate of reradiating volume
S = Path length for radiation exchange to control volume, m
S' = Path length for radiation exchange to absorbing medium, m
T = Temperature of argon, K
T_0 = Entry gas temperature, K
$T_{particles}$ = ZnO particle phase temperature, K
T_{wall} = Outer wall temperature, K
$\vec{t}$ = Unit vector tangential to boundary
$\dot{V}_{bottom}$ = Inlet volumetric flowrate at bottom annular inlet, m^3 s^{-1}
$\dot{V}_{central}$ = Inlet volumetric gas flowrate at central region inlet, m^3 s^{-1}
$\dot{V}_{gas}$ = Inlet volumetric gas flowrate, m^3 s^{-1}
$\dot{V}_i$ = Inlet volumetric flowrate at boundary i, m^3 s^{-1}
$\dot{V}_{top}$ = Inlet volumetric flowrate at top annular inlet, m^3 s^{-1}
$\vec{v}$ = Argon gas velocity vector, m s^{-1}
X = Fractional conversion of ZnO
z = Diffusion distance from the particle surface to bulk gas, m
z_0 = Axial coordinate of point on system boundary
z^* = Axial coordinate of re-radiating volume

Greek letters

δ_{ij} = Kroenecker delta
ΔH°_T = Standard enthalpy of dissociation of ZnO at temperature T, J mol^{-1}

ΔS_T° = Standard entropy of dissociation of ZnO at temperature T, J mol^{-1} K^{-1}
ε = Void fraction in the porous section
ε_{porous} = Emissivity of the porous section
λ = Wavelength, m
μ = Argon viscosity, kg m^{-1} s^{-1}
ν = Number of moles of gas generated by dissociation of 1 mol of solid
ρ = Gas density, kg m^{-3}
ρ_{ZnO} = Bulk density of ZnO, kg m^{-3}
$\rho_{ZnO,eff}$ = Effective density for ZnO particle phase, kg m^{-3}
σ = Characteristic diameter of gas molecule, m
σ_{O_2-Ar} = Mean characteristic diameter of oxygen and argon, m
σ_{sb} = Stefan–Boltzmann constant, W m^{-2} K^{-4}
σ_λ = Scattering coefficient, m^{-1}
$\vec{\vec{\tau}}$ = Viscous stress tensor, kg m^{-1} s^{-2}
τ_{ij} = (i,j) component of viscous stress tensor, kg m^{-1} s^{-2}
$\Phi(\lambda,\omega)$ = Scattering phase function
φ_0 = Azimuthal coordinate of point on system boundary
φ^* = Azimuthal coordinate of radiating volume
Ω = Viscosity–thermal conductivity collision integral for argon
Ω_{O_2-Ar} = Diffusion collision integral for oxygen in argon
ω = Unit solid angle, steradians

Literature Cited

1. Steinfeld A. Solar hydrogen production via a two-step water-splitting thermochemical cycle based on Zn/ZnO redox reactions. *Int J Hydrogen Energy*. 2002;27:611–619.
2. Dahl J, Buechler K, Weimer A, Lewandowski A, Bingham C. Solar-thermal dissociation of methane in a fluid-wall aerosol flow reactor. *Int J Hydrogen Energy*. 2004;29:725–736.
3. Matovich E. High temperature chemical reaction processes utilizing fluid-wall reactors. U.S. Pat. No. 4095974.
4. COMSOL Multiphysics, Version 3.2. Sweden: COMSOL AB, 2006.
5. Lide D, editor. *CRC Handbook of Chemistry and Physics*, 74th ed. Boca Raton: CRC, 1993.
6. Bird RB, Stewart WE, Lightfoot, EN. *Transport Phenomena*, *1st ed*. New York: Wiley, 1960.
7. Hinds WC. *Aerosol Technology: Properties, Behavior, and Measurement of Airborne Particles*, *1st ed*. New York: Wiley, 1999.
8. Ingham DB, Pop II. *Transport Phenomena in Porous Media*, *1st ed*. Danvers, MA: Pergamon, 1998.
9. Scheidegger AE. *The Physics of Flow through Porous Media*, *1st ed*. Toronto: University of Toronto Press, 1960.
10. Kaviany M. *Principles of Heat Transfer in Porous Media*, *1st ed*. New York: Springer-Verlag, 1991.
11. Crystal Purity and Material Properties, 2006. Saint-Gobain Industrial Ceramics. http://www.crystar.com/media/documents/s0000000000000001009/Purity_Material_Prop.pdf
12. L'vov B. Interpretation of atomized mechanisms in electrothermal atomic absorption spectrometry by analysis of the absolute rates of the processes. *Spectrochemica Acta Part B* 1997;52:1–23.
13. Moller S, Palumbo R. Solar thermal decomposition kinetics of ZnO in the temperature range 1950–2400 K. *Chem Eng Sci* 2001;56:4505–4515.
14. Perkins C. *Solar Thermal Decomposition of Zno in Aerosol Flow for Renewable Hydrogen Production*, Ph.D. Thesis, University of Colorado, 2006.
15. Weidenkaff A, Reller A, Wokaun A, Steinfeld A. Thermogravimetric analysis of the ZnO/Zn water splitting cycle. *Thermochim Acta* 2000;359:69–75.
16. Siegel R, Howell JR. *Thermal radiation heat transfer*, *3rd ed*. Washington, DC: Taylor & Francis, 1992.
17. Bohren CF, Huffman DR. *Absorption and scattering of light by small particles*, *ed*. 1st edition, New York: Wiley-Interscience, 1983.
18. Liu Y, Hsieh J, Tung S. Extraction of optical constants of zinc oxide thin films by ellipsometry with various models. *Thin Solid Films* 2006;510:32–38.
19. Coulson J, Richardson J. *Chemical Engineering: Fluid Flow, Heat Transfer, and Mass Transfer*, *6th ed*. Oxford: Butterworth-Heinemann, 1999.
20. Aref'ev KM, Balashova NB, Guseva MA, Zhilin AV. Diffusion of vapors of metals of group II in inert gases, nitrogen, and hydrogen. *High Temp* 1995;33:142–145.
21. Francis T, Gump C, Weimer A. Spinning wheel powder feeding device—fundamentals and applications. *Powder Technol* 2006;170:36–44.
22. Dahl JK, Buechler KJ, Finley R, Stanislaus T, Weimer AW, Lewandowski A, Bingham C, Smeets A, Schneider A. Rapid solar-thermal dissociation of natural gas in an aerosol flow reactor. *Energy* 2004;29:715–725.

Manuscript received Oct. 25, 2006, and revision received Apr. 2, 2007.